PPPL-2324

UC20-G

PPPL-2324

CALCULATION OF COUPLING TO SLOW AND FAST WAVES IN THE LHRF FROM PHASED WAVEGUIDE ARRAYS

By

R.I. Pinsker, R.E. Duvall, C.M. Fortgang, and P.L. Colestock

APRIL 1986

PLASMA PHYSICS LABORATORY

PRINCETON UNIVERSITY

PRINCETON, NEW JERSEY

PREPARED FOR THE U.S. DEPARTMENT OF ENERGY, UNDER CONTRACT DE-AC02-76-CHO-3073.

PPPL--2324

DE86 009752

Calculation of Coupling to Slow and Fast Waves in the LHRF from Phased Waveguide Arrays

R. I. Pinsker, R. E. Duvall, C. M. Fortgang, and P. L. Colestock
Plasma Physics Laboratory, Princeton University
Princeton, NJ 08544

ABSTRACT

A previously reported algorithm for solving the problem of coupling electromagnetic energy in the LHRF from a phased array of identical rectangular waveguides to a plane-stratified, magnetized cold plasma is numerically implemented. The resulting computer codes are sufficiently general to allow for an arbitrary number of waveguides with finite dimensions in both poloidal and toroidal directions, and are thus capable of computing coupling to both slow and fast waves in the plasma. Some of the details of the implementation and the extension of the algorithm to allow study of the Fourier spectrum of slow and fast waves launched by the array are discussed. Good agreement is found with previously reported, less general work for the slow wave launching case. The effect of phasing multirow arrays in the poloidal direction is studied, and an asymmetry between phasing 'up' and 'down' is found that persists in the case where the plasma adjacent to the array is uniform. A 4×3 array designed to launch fast waves of high phase velocity is studied. By using the optimal poloidal phasing, low reflection coefficients ($|R|^2 \lesssim 20\%$) are found under some not unrealistic edge plasma conditions, but most of the input power is trapped in the outermost layer of the plasma. Implications of our results for fast wave current drive experiments are discussed.

1. INTRODUCTION

In the past decade, plasma waves in the *Lower Hybrid Range of Frequencies* ($\Omega_i \ll \omega \sim \omega_{pi} \ll \Omega_e$) have experimentally been proven to be effective for plasma current drive and heating [1,2] . While several types of wave launching structures have been employed in small, low power experiments, the antenna design used for high power tokamak experiments in the *LHRF* is the phased waveguide array. The simplicity and flexibility of these antennas has led to their important role in recent tokamak reactor designs [3] .

From a practical point of view, the maximum amount of power which can be delivered to the plasma by a phased waveguide array can be limited by the appearance of significant reflection at the array–plasma interface; high voltage standing waves in the guides can cause breakdown in the guides. Consequently, it is important to be able to predict the reflection coefficients as a function of plasma conditions in front of the array. Furthermore, the layer of plasma in front of the array, which we will henceforth call the coupling region, acts as a filter, only permitting part of the launched power spectrum to reach the core of the plasma. The detailed spectrum of the waves that reach the hot plasma core is clearly important for wave absorption, and hence for heating and current drive.

For these reasons, a theory to describe waveguide array–plasma coupling has been developed and implemented in the form of computer codes [4–6] . These codes are limited to modelling arrays composed of rectangular guides with the shorter edge parallel to the toroidal field (slow wave coupler), and treat coupling only to the slow wave [7] . The results of these codes have been compared in some detail with slow wave launching experiments [8,9] . *Ref. 10 includes the* parasitic coupling to the fast wave from a slow wave coupler, while Theilhaber and Bers [11] consider coupling to the fast wave with an array of guides with the longer edge parallel to the toroidal field (fast wave coupler). All of this work shares a set of assumptions: plane–stratified cold plasma in the coupling region, special density profiles that can be treated analytically, arrays of infinite

extent in the poloidal direction so that the poloidal wave number is zero, and decoupled differential equations describing slow and fast wave propagation.

Berger, Perkins, and Troyon [12] and McWilliams and Mok [13] have considered the effect of nonzero poloidal wave number on fast wave propagation, and in Ref. 13 arbitrary density profiles were allowed as well. In both of these studies, however, it was assumed that the antenna launched one particular plane wave at a time, and thus these authors did not match the fields at the plasma edge to those of a realistic coupler. Furthermore, these studies also decoupled the slow and fast wave differential equations.

While the assumptions made in all of these studies are well justified for slow wave launching, as we shall see below, they are not as justifiable for fast wave launching. The finite poloidal extent of the array is more significant for the fast wave case, and the launching of high phase velocity fast waves for efficient current drive will necessarily involve relatively large amounts of power in the inaccessible part of the wave spectrum. (Of course, the latter point is true for the launching of high phase velocity slow waves as well.) For the waves near the minimum accessible wave number, the assumptions which allow decoupling of slow and fast wave differential equations break down. Also, phasing the array poloidally may allow much improved coupling efficiency to the fast wave, as was emphasized in Ref. 13 .

Bers and Theilhaber [14] outlined a computational method which allows the removal of most of these assumptions, though no numerical work was reported. The following approximations remain: the plasma is plane-stratified, the DC magnetic field is purely toroidal, and the coupling region is treated using cold plasma theory. Other assumptions will be discussed below. The density and toroidal field profiles are arbitrary, the slow and fast wave differential equations do not have to be decoupled, and the array is of finite extent in both poloidal and toroidal directions. This method has been implemented to treat coupling from a single large waveguide to the plasma for the *Ion Cyclotron Range of Frequencies* [15] . In the present work, we implement this method for the LHRF and use the resulting code to study waveguide array–plasma coupling using an array

designed for a fast wave current drive experiment [16] .

The organization of the paper is as follows. In Sec. 2, we discuss the details of the implementation of this numerical scheme. The next section discusses a comparison of the results of our code with the results of a slow wave coupling code which has been previously described [5] , and presents results from a study of fast wave launching with a 4×3 phased array. An asymmetry between coupling obtained with 'up' and 'down' poloidal phasing, which exists even if the plasma in the coupling region is uniform, is discussed. The Fourier spectrum of slow and fast waves launched by the array is studied. We list our conclusions in Sec. 4.

2. NUMERICAL METHODS

The method we use to calculate waveguide array–plasma coupling has been described in detail in several previous publications [10,14,15] , so the following discussion emphasizes the aspects of the present work which are new or have not been previously described. The model array consists of an arbitrary number of identical rectangular waveguides loaded with dielectric. The dimensions of the guides are such that only the TE_{01} or TE_{10} mode propagates at the excited frequency, but an arbitrary number of evanescent TE and TM modes may be retained in the coupling calculation. The coordinate system used is illustrated in Fig. 1. Apart from the waveguide apertures, the $x = 0$ plane consists of a perfectly conducting sheet, so that the transverse electric field vanishes everywhere on $x = 0$ except in the waveguide openings. Since the number and dimensions of the waveguides are finite in both the y and z directions, we can investigate the effect of phasing the array in the direction perpendicular to $\mathbf{B}_0$.

The Fourier transform of the transverse electric field in the plasma matches onto the transform of the waveguide fields at $x = 0$. The transverse magnetic fields match only in the waveguide openings, so that one cannot simply match the Fourier–transformed transverse magnetic fields at $x = 0$. The transforms of the transverse electric and magnetic fields at $x = 0^+$ are related by the

admittance matrix $\mathbf{Y}(n_y, n_z)$ defined by

$$\begin{pmatrix} B_y(x=0^+, n_y, n_z) \\ B_z(x=0^+, n_y, n_z) \end{pmatrix} = \begin{pmatrix} Y_{11}(n_y, n_z) & Y_{12}(n_y, n_z) \\ Y_{21}(n_y, n_z) & Y_{22}(n_y, n_z) \end{pmatrix} \begin{pmatrix} E_y(x=0^+, n_y, n_z) \\ E_z(x=0^+, n_y, n_z) \end{pmatrix}. \tag{1}$$

(In this paper, we normalize wave numbers by the vacuum wave number $k_0 = \omega/c$, thus defining the index of refraction in the y-direction, for example, as $n_y \equiv k_y/k_0 = k_y c/\omega$.) The admittance matrix is calculated in the manner described by Refs. 14 and 15 : for a particular (n_y, n_z), the polarizations of the pure slow and fast modes are calculated in the plasma at a point sufficiently far to the right that a radiation condition applies. That is, the modes carry energy only towards the right, away from the launching structure. If for this (n_y, n_z) a mode is evanescent and therefore carries no energy towards the right, the solution which decays towards the right is chosen. These two solutions are then taken in turn as initial conditions for the integration back to $x = 0^+$ of Maxwell's equations incorporating the linear cold plasma dielectric tensor. These four coupled, first order ordinary differential equations include the x dependence of the electron density and B_z, and the terms involving spatial derivatives of dielectric tensor elements are retained. This integration yields the electric and magnetic fields at $x = 0^+$, from which the following set of four equations for the four unknown admittance matrix elements may be constructed:

$$\begin{aligned}
B_y^{fast}(x=0^+, n_y, n_z) &= Y_{11}(n_y, n_z) E_y^{fast}(x=0^+, n_y, n_z) + Y_{12}(n_y, n_z) E_z^{fast}(x=0^+, n_y, n_z) \\
B_z^{fast}(x=0^+, n_y, n_z) &= Y_{21}(n_y, n_z) E_y^{fast}(x=0^+, n_y, n_z) + Y_{22}(n_y, n_z) E_z^{fast}(x=0^+, n_y, n_z) \\
B_y^{slow}(x=0^+, n_y, n_z) &= Y_{11}(n_y, n_z) E_y^{slow}(x=0^+, n_y, n_z) + Y_{12}(n_y, n_z) E_z^{slow}(x=0^+, n_y, n_z) \\
B_z^{slow}(x=0^+, n_y, n_z) &= Y_{21}(n_y, n_z) E_y^{slow}(x=0^+, n_y, n_z) + Y_{22}(n_y, n_z) E_z^{slow}(x=0^+, n_y, n_z)
\end{aligned} \tag{2}$$

in which the superscript denotes which solution was taken as initial condition at the far right. The solution of this set yields $\mathbf{Y}(n_y, n_z)$. This procedure must be carried out for enough points in the (n_y, n_z) plane to allow the inverse Fourier

transform integrals to be computed accurately. The radius in the (n_y, n_z) plane out to which the inverse Fourier transform integrals are calculated is determined by the launched spectrum of the array; the circle must include all the significant energy launched by the array. (This is certainly sufficient for the present coupling calculation, but for detailed current drive studies, the exponentially small amounts of launched energy at large values of $|n_z|$ may partially fill in the 'velocity gap' [17] .)

In the integration of Maxwell's equations in the plasma, several numerical problems may arise. Starting in the high density region at the right with a unit amplitude mode, the wave amplitude may grow to a value larger than the precision of the computer if the wave is evanescent in the lower density to the left. If one of the modes is much more evanescent than the other, the equations are 'stiff' [18] . In the LHRF, the density below which the slow wave is evanescent is approximately

$$n_e|_{crit}^{slow} \simeq \frac{m_e}{4\pi e^2}\omega^2(n_y^2 + n_z^2 - 1)/(n_z^2 - 1)$$

for $n_z^2 > 1$, while the fast wave is roughly as evanescent as it is in vacuum $(n_x \simeq i(n_y^2 + n_z^2 - 1)^{1/2})$ for densities below

$$n_e|_{crit}^{fast} \simeq \frac{m_e}{4\pi e^2}\omega\Omega_e(n_y^2 + n_z^2 - 1)^{1/2}(n_z^2 - 1)^{1/2}.$$

For $n_y = 0$, we see that

$$\frac{n_e|_{crit}^{fast}}{n_e|_{crit}^{slow}} \simeq \frac{\Omega_e}{\omega}(n_z^2 - 1) \gg 1 ,$$

except for a narrow range of $n_z^2 \gtrsim 1$. Further, waves for which the high density region at the far right is inaccessible undergo exponential growth towards the left until the mode conversion point is reached. The spatial growth rate in the plasma to the right of the mode conversion point can be much larger than the growth rate in the low density region near $x = 0^+$.

Our algorithm for dealing with these difficulties proceeds as follows. After an integration of Maxwell's equations, the ratio of the field magnitudes at $x = 0^+$

to the magnitude at the start of the integration at $x = x_{right}$ is computed. If this ratio is larger than 10^8, then the WKB dispersion relation is examined at all points between $x = 0^+$ and $x = x_{right}$ to search for mode conversion points, i. e. , points where the two roots for $n_x^2(x, n_y, n_z)$ coalesce. Upon finding such a point, the integration is restarted one quarter of a local wavelength to the right of the leftmost mode conversion point. If no mode conversion point is found, or if the new integration still results in a ratio greater than 10^8, the problem was due not to the presence of a mode conversion layer, but to evanescence at low density. In this case, the integration is restarted at $x = x_{right}/2$. Each time the integration is restarted at a new point, the two polarizations which carry energy towards the right or decay towards the right must be recalculated at the new starting point. The error incurred by neglecting the waves which carry energy towards the left or decay towards the left is exponentially small, since these waves represent reflections from higher density further to the right and therefore are reduced in amplitude by a factor of $\exp(-2\int_{x_{new}}^{x_{ref}} \mathrm{Im}(n_x)dx)$, where x_{new} is the new starting point and x_{ref} is the reflection point at the right. Note that $x_{new} < x_{ref} < x_{right}$. Amending the basic technique for calculating the admittance matrix in this way, we find that in the LHRF we need not resort to decoupling the differential equations for fast and slow waves, as was done for the ICRF in Ref. 15 . Had this decoupling been required in the LHRF, the utility of the numerical method would have been questionable, as the launching of high phase velocity waves for efficient current drive inevitably entails the launching of significant power into the inaccessible part of the spectrum. These waves undergo mode conversion within the coupling region, and the accuracy of any decoupling scheme will, of course, break down in the neighborhood of the mode conversion points, where the two polarizations are indistinguishable.

A different numerical difficulty arises when calculating inverse Fourier transform integrals. As discussed in Ref. 10 , several kinds of standing waves in the coupling region lead to singularities in the Y matrix elements which occur for certain real values of (n_y, n_z). For simplicity in the following discussion, let us temporarily suppose that $n_y = 0$, and find the contour in the complex k_z plane

for the inverse Fourier transform integration. The manner in which this path avoids the singularities on the real axis is dictated by causality. The method used to determine the correct contour is exactly analogous to the standard technique used to resolve a similar difficulty in the Landau problem [19] . In the Landau problem, an integral over velocity has a singularity occurring in the integrand on the path of integration. The correct way to circumnavigate the singularity is found by treating the problem as an initial value problem, employing the Laplace transform in time, and requiring that the solution be causal.

In the present problem, the singularities occur when computing an integral over k_z. To determine the correct contour, then, we consider the initial value problem, wherein the forward propagating waveguide mode of frequency $\omega = \omega_{excited}$ is 'turned on' at $t = 0$. If we take the Laplace transform in time, the integration path in the complex ω plane for the inverse Laplace transform runs above the real ω axis, since the excited mode yields a singularity on the real ω axis at $\omega = \omega_{excited}$. We next invert the Fourier transform, before inverting the Laplace transform. Consider a singularity in the $\mathbf{Y}$ matrix occurring at $n_z = n_{z0}$. A singularity in the inverse Fourier transform integrand then occurs at $k_z = (\frac{\omega}{c})n_{z0}$. Since we introduced a positive imaginary part to ω for causality, and we take $\mathrm{Re}(\omega) > 0$, then $\omega \rightarrow |\omega| \exp(i\theta)$ with $\theta > 0$. Then the singularity occurs at $k_z = (n_{z0}/c)|\omega| \exp(i\theta)$, i. e. , the singularity has been rotated counterclockwise off the real k_z axis. The path for the inverse Fourier transform coincides with the real k_z axis, and does not encounter any singularities. But as we let $\mathrm{Im}(\omega) \rightarrow 0$ from above, the singularities in the complex k_z plane rotate back towards the real axis. Then the unique analytic continuation of the inverse Fourier transform requires that the path be distorted so as to run above the singularities on the negative real k_z axis and below the singularities on the positive real k_z axis.

A simple example should clarify this. The singularities of the $\mathbf{Y}$ matrix elements for a vacuum are of the form $(1 - n_z^2)^{-1/2}$ (with $n_y = 0$). In this case, the singularities occur at $k_z = (\pm 1/c)|\omega| \exp(i\theta)$. The inverse Fourier transform path and the branch cuts are illustrated in Fig. 2a. Then as $\mathrm{Im}(\omega) \rightarrow 0$ from above, the branch cuts rotate back to the real k_z axis, and the path must be

deformed as shown in Fig. 2b. Finally, from this point on, we consider $\mathrm{Im}(\omega) = 0$ so that the path in the complex n_z plane is of the same form as the path we have found in the k_z plane. Identical conclusions concerning this contour have been reached by Brambilla [4] and Theilhaber and Bers [11] . In practice, we follow this prescription by giving n_z (and, analogously, n_y) in the Maxwell equations a small imaginary part as follows: for $n_z < 0$, $n_z \rightarrow n_z + i|\epsilon|$, and for $n_z \geq 0$, $n_z \rightarrow n_z - i|\epsilon|$. Thus, the $\mathbf{Y}$ matrix which we find by integrating these equations is evaluated along the contour shown in Fig. 2c. We take $|\epsilon| \ll 1$ because we have replaced only the n_z that appears in $\mathbf{Y}$ with this complex value; the other factors involving n_z that multiply the elements of $\mathbf{Y}$ in the inverse Fourier transform integrals are entire functions of n_z, so that we are effectively carrying out the integrals along the path described.

After the inverse Fourier transforms have been carried out, one is left with a matrix inversion which finally yields the "scattering matrix" [20] . This matrix connects the incident and reflected amplitudes of each mode in each waveguide. Once this matrix is obtained for a particular density profile, B_z profile, etc., the reflection coefficients of each mode in each guide for any incident phasing in the z (toroidal) and y (poloidal) directions may be trivially calculated by a single matrix multiplication. Furthermore, one may find the launched spectrum of slow and fast waves at any given x between $x = 0^+$ and $x = x_{right}$ with the expenditure of a relatively small amount of computer time. This enables us to compute, for example, the amount of power launched into the slow mode by a nominal fast wave coupler (long edges of the guides parallel to $\mathbf{B}_0$).

To carry out this decomposition of the wave power spectra into slow and fast modes, the following elaboration of the method described above is used. For each (n_y, n_z) of interest, pure slow and fast waves of unit amplitude in the plasma region at the far right are integrated backwards across the density profile as before. At each intermediate x position at which the spectra will be desired, the field values are stored. Having already solved the coupling problem, the actual value of the transverse electric field at $x = 0^-$ is known for a given array phasing from the scattering matrix. The condition that the Fourier transform

of the transverse electric field matches at $x = 0$ yields the amplitudes of the two initial conditions, i. e. , the mixture of slow and fast waves at the far right, both of which satisfy a radiation condition there, that give the correct fields at $x = 0$. At each x position, then, the actual launched fields are known. At each such point, we may define a rightgoing fast wave, a leftgoing fast wave, a rightgoing slow wave, and a leftgoing slow wave in terms of a hypothetical uniform plasma, the parameters of which are everywhere the same as the plasma at that x position. The actual fields may be broken up into a sum of these four eigenvectors; the four transverse field components give exactly the necessary amount of information to carry out this decomposition.

3. RESULTS AND DISCUSSION

To benchmark our code, we compared its results with those of a code described by Stevens *et al.*[5] . The array consisted of four guides driven at 2 GHz, each 2 cm wide and 13 cm high, separated by 0.3 cm, arranged with the narrow edge along the z direction (slow wave coupler). For the Stevens code, the ion mass and the toroidal field strength B_0 are irrelevant due to the approximations used, while for our code we took the working gas to be deuterium and $B_0 = 20$ kG. The density profile consisted of a ramp starting at 1.5×10^{11} cm^{-3} at $x = 0^+$ rising with a gradient of 2×10^{11} cm^{-4}. While the Stevens code retains no evanescent waveguide modes, we kept two evanescent TE modes and the evanescent TM_{11} mode.

The results of the comparison are displayed in Figs. 3 and 4. The reflection coefficient in each of the four guides as a function of the phasing angle is compared, as is the net transmission coefficient for the array. The agreement is satisfactory. The outer two guides have lower reflections than the inner two at phase angles near 180° because the outer two have neighboring guides on only one side, and therefore act more like a single waveguide [5] . The spectrum excited by a single guide is peaked around $n_z = 0$ and therefore matches best to a vacuum, in which only waves with $|n_z| < 1$ propagate. The inner two guides

couple best at an edge density of 5×10^{11} cm^{-3}, since at a phasing of 180° the spectrum is peaked at $n_z \simeq 3.3$ and, according to Ref.5, optimal coupling occurs at a density of $n_{opt} = n_{crit}\, n_z^2 = (5 \times 10^{10}\ \mathrm{cm}^{-3})(3.3)^2$. Since the edge density in this example is much less than the optimal density, the outer two guides couple better than the inner two. Similarly, for phase angles near 0° the outer guides have lower reflections than the inner two, because the width of the peak at $n_z = 0$ for a single guide is greater than that of an array phased at 0°, so the spectrum of a single guide has a smaller proportion of energy in the inaccessible range of wave numbers. Other qualitative features of coupling from a slow wave array to a plasma with the type of density profile in this example are discussed in detail in Ref.5 .

In the next example, we consider coupling from a fast wave array. We model the array to be used for the PLT fast wave current drive experiment [10] . twelve guides driven at 800 MHz, each 8.6 cm in the toroidal direction by 5.4 cm in the poloidal direction, arrayed in four columns of three. The septum between the guides toroidally is 0.67 cm, and the poloidal separation is 2.9 cm. The guides are filled with a dielectric with $\epsilon = 8.0$. As is well known, to obtain reasonable coupling efficiency to the fast wave in the LHRF, a relatively high density is required. We therefore take the density at the limiter (located at $r = 40$ cm) to be $n_{lim} = 5 \times 10^{12}$ cm^{-3}, rising parabolically over 40 cm to a central density of $n_0 = 5 \times 10^{13}$ cm^{-3}, and an exponential decay of the density from the limiter radius outwards with an e–folding distance of 2 cm. This 'standard' density profile is shown in Fig. 5. The $1/R$ variation of the toroidal field, which is taken to be $B_0 = 20$ kG at the array face, is included, although this amounts to an increase of B_z of only 6% over the 10 cm we take to constitute the coupling region. The working gas is deuterium.

We now investigate the effect of moving the position of the array from its nominal position 3 cm outside the limiter, with a fixed phasing and density profile. The phasing is chosen to be 90° in the toroidal direction and 0° in the poloidal direction. The resulting power reflection coefficient is plotted as a function of the distance between the array face and the limiter in Fig. 6. An

optimum density at the array face exists, of about 1.8×10^{12} cm^{-3}, at which the reflection coefficient is about 44%. However, as suggested by McWilliams and Mok [13] , the coupling may be improved significantly by poloidally phasing the array. With a 90° phase difference of the appropriate sign between adjacent guides in the y–direction while maintaining the 90° phase difference in the z–direction, the lower reflection coefficients also plotted in Fig. 6 are obtained. The reflection coefficients with the optimum poloidal phasing are considerably lower than those with zero poloidal phasing for all array positions; at the nominal position, 22% power reflection is obtained in the former case, compared with 46% in the latter.

We further investigate the effect of poloidal phasing by fixing the array face position at its nominal value of $r = 43$ cm, maintaining the toroidal phasing of 90°, and varying the poloidal phasing from −180° to 180°. (As noted in Sec. 2, having found the "scattering matrix," the reflection coefficient for any phasing is found by a single matrix multiplication.) The power reflection coefficient thus found is plotted in Fig. 7a. The reflection coefficient is strongly dependent on the sign of the poloidal phase angle, with the optimum occurring at about −70° This asymmetry is in contrast to the dependence of the reflection coefficient on the toroidal phase angle with fixed poloidal phase; such a plot, with the fixed poloidal phase angle of 0°, is shown in Fig. 7b. We may display the reflection coefficient for any phasing in both directions by plotting contours of constant power reflection in "phasing angle space." The power reflection contour plot for the standard case under discussion here is shown in Fig. 8. The z–phasing symmetry and the y–phasing asymmetry are immediately obvious in this plot.

Another interesting feature of Fig. 8 is generally found for density profiles and toroidal field strengths such that good coupling ($|R|^2 \sim 30\%$ or less) exists for some phasing: the minimum reflection coefficient is achieved for a particular y–phasing, but does not strongly depend on the z–phase angle. This is displayed in Fig. 7c, which shows the reflection coefficient as a function of z–phasing angle with the y–phasing angle fixed at −90°. The existence of an optimal poloidal phasing at which not only the minimum reflection coefficient is obtained, but

at which the toroidal phase angle can be varied across a wide range without adversely affecting the coupling efficiency, is of obvious significance for fast wave current drive experiments.

However, the mechanism by which poloidal phasing improves coupling in this case is not primarily the one described by Berger, Perkins, and Troyon [12] and McWilliams and Mok [13] , which involves the spatial derivative of the off–diagonal plasma dielectric tensor elements. This is demonstrated by recomputing the standard case, replacing the density and B_z profiles by a uniform plasma with parameters n_e and B_0 equal to their values at $x = 0^+$ in the standard case: $n_e = (5 \times 10^{12}\ \mathrm{cm}^{-3}) \times \exp(-3\ \mathrm{cm}/2\ \mathrm{cm}) = 1.1 \times 10^{12}\ \mathrm{cm}^{-3}$, and $B_0 = 20$ kG. The power reflection coefficient contours are shown in Fig. 9. Though all the gradients in the plasma are now zero, the effect of poloidal phasing remains substantially the same as with the realistic density profile.

The strong asymmetry between phasing 'up' and 'down' which is apparent in Fig. 9 may at first appear to be counterintuitive; in a uniform magnetized plasma with a straight magnetic field, no direction perpendicular to the magnetic field is preferred. However, a 'uniform' plasma bounded by a conducting sheet is manifestly not truly uniform, in that the normal to the sheet ($\hat{x}$), the magnetic field direction ($\hat{z}$), and their cross product form a basis with a particular handedness, with respect to which an unique 'up' direction is defined. For fast wave launching into a uniform plasma, this effect may be seen more explicitly by approximating $\mathbf{E} \cdot \hat{z} \simeq 0$, which is the usual decoupling assumption for fast waves [13,15] , in which case the relevant admittance matrix element $Y_{21}(n_y, n_z)$ is given by [15]

$$Y_{21} \approx \frac{B_z}{E_y} = \frac{n_x^{fast}(S - n_z^2) - iDn_y}{S - n_z^2 - n_y^2} \quad , \tag{3}$$

in which $n_x^{fast} = n_x^{fast}(x, n_y, n_z)$ is the index of refraction for the fast wave in the x–direction. For n_y, n_z such that $\mathrm{Im}(n_x^{fast}) \neq 0$ (evanescent waves), this is clearly asymmetric with respect to the interchange $n_y \rightarrow -n_y$. Thus, the reactive part of the plasma impedance depends on whether the array is phased 'up' or 'down' for a uniform plasma.

If the antenna structure is idealized so that a single plane wave with a particular (n_y, n_z) is launched, as it was in Refs. 12 and 13, no asymmetry between coupling with $n_y = +n_{y0}$ and $n_y = -n_{y0}$ will be observed for a uniform plasma, because for propagating waves Eq. (3) shows that the magnitude of Y_{21} is unchanged under the interchange $n_y \rightarrow -n_y$, while the evanescent waves which introduce the asymmetry carry no energy away from the antenna. It is the constraint that the fields at the edge of the plasma must match onto the fields of a realistic antenna model which forces the launching of evanescent waves into the plasma along with the propagating waves, and the evanescent waves introduce the up–down asymmetry. That evanescent waves are required to be able to match the plasma and waveguide fields is most obvious for a single mode in a single waveguide: the ratio of incident power in the evanescent part of the spectrum to that in the propagating part is fixed for this case.

At the high plasma densities contemplated for fast wave current drive, coupling to slow waves of high phase velocity becomes difficult. This may be anticipated from the rule–of–thumb of Ref. 5 mentioned above: at 800 MHz, the optimal edge density for coupling at $n_z = 1.5$ is predicted by this formula to be $n_e^{opt} \simeq 1.8 \times 10^{10}$ cm^{-3} , while the density at the array face for our standard profile with the array 5 cm outside the limiter is 4.1×10^{11} cm^{-3}. To make a quantitative comparison between slow– and fast–wave coupling with the same density and B_z profiles, etc. , we model the 6×1 waveguide array formerly used in PLT lower hybrid current drive experiments at 800 MHz [21] . Each guide is 3.53 cm wide and 22 cm high, and the guides are separated by 0.63 cm in the toroidal direction.

Fixing the toroidal phase angle at 90°, the incident power spectrum of this array is peaked at $n_z^{peak} \simeq 2.25$, with a half–width–at–half–maximum of $(\Delta n_z)_{HWHM} \sim 1$. The array face would have to be located approximately 10 cm outside the limiter, given our standard density profile, to obtain optimal coupling. The reflection coefficient for this array as a function of the distance between the array face and the limiter is plotted in Fig. 10. Comparison of Figs. 6 and 10 shows that with proper poloidal phasing, the 4×3 fast wave

coupler can achieve lower reflection coefficients than the slow wave array. This is further illustrated in Fig. 11, wherein the reflection coefficients for both arrays are compared as a function of toroidal phase angle. For this comparison, the arrays are both located 3 cm outside the limiter, and the poloidal phase angle for the fast wave array is fixed at $-70°$ (near the optimal value for 90° toroidal phasing).

The dependence of coupling on the toroidal field strength B_0 is quite different for the slow– and fast–wave arrays. The cut–off condition for the slow wave is independent of magnetic field, but at very low field and high edge density, the accessibility condition becomes difficult to satisfy. Under these conditions, most of the incident slow wave energy undergoes mode conversion to the fast wave in the outer part of the plasma and does not escape the coupling region. The cut–off condition for the fast wave, on the other hand, depends on the magnetic field, so that low magnetic fields are favorable for good fast wave coupling. At very low field, however, the same accessibility criterion makes coupling difficult. Hence, one expects that an optimal B_0 exists for fast wave coupling, while for field strengths above some value B_0^{crit}, slow wave coupling will not depend on B_0. For the 6×1 slow wave coupler, we may estimate this critical B_0 by calculating the field at which most of the spectral energy is accessible. At 90° phasing, most of the incident energy is above $n_z = n_z^{peak} - (\Delta n_z)_{HWHM} \simeq 1.25$, which is accessible to a density of 1.1×10^{12} cm^{-3} for $B_0 \gtrsim 15$ kG. The power reflection coefficient for the slow wave array as a function of B_0 is shown in Fig. 12, where the array face is 3 cm outside the limiter, the density profile of Fig. 5 is used, and the toroidal phasing is 90° . The reflection coefficient is indeed independent of B_0 above $B_0^{crit} \sim 15$ kG. Fig. 13 shows the dependence of reflection coefficient for the 4×3 fast wave array on B_0 for the standard case, with a toroidal phasing of 90° and two poloidal phasing angles. The anticipated minimum in reflection coefficient is seen to exist; for poloidal phasing of $-90°$, the minimum reflection coefficient is approximately 15% at $B_0 \simeq 10$ kG.

Finally, we use our methods to consider the nature of the wave spectrum that actually escapes the coupling region. The relatively low reflection coeffi-

cients here obtained for fast wave launching do not necessarily imply that large amounts of power are able to reach the plasma core; power trapped between the edge of the plasma and the mode conversion points may only weakly affect the reflection coefficient of the array, but is useless for heating or driving current in the plasma beyond the coupling region. Further, for current drive experiments, it is necessary to know the polarization of the wave energy that does escape the coupling region. Under some conditions, fast wave arrays can launch significant amounts of power into the slow wave branch both by direct coupling from evanescent waveguide modes (excited by the matching at $x = 0$) or by coupling across the density gradient. The mechanism by which the latter coupling can occur has been described by Skiff [22] for the similar situation wherein the fast wave in the ICRF couples to the ion Bernstein wave.

As Brambilla [10] has discussed in detail, power trapped in the coupling region between mode conversion points and the plasma edge causes narrow peaks to appear in the inaccessible part of the Fourier spectrum of the x–component of the Poynting flux $P_x(n_y, n_z)$. The peaks have nonzero width only if some damping mechanism exists, allowing power flowing in the z–direction to vanish at large distances from the antenna. Our introduction of an imaginary part to n_y and n_z has the same effect as the introduction of an imaginary part to a phase integral in Ref. 10, so that the power spectrum at $x = 0^+$ has the fine structure just described. As the spectrum is calculated at $x > 0^+$, the power in the inaccessible part of the spectrum decreases until at $x = x_{right}$, where only waves carrying energy towards the right or decaying towards the right are permitted, only an exponentially small part of the power in this part of the spectrum has tunnelled through.

We may calculate the fraction of inaccessible power either by computing the volume under this part of the power spectrum at $x = 0^+$, or by computing the power at $x = x_{right}$ and subtracting this from $P_{inc}(1 - |R|^2)$, where P_{inc} is the total power propagating towards the right in the array and $|R|^2$ is the power reflection coefficient for the array. The latter scheme is clearly easier to numerically implement and is also more accurate. However, the full two–

dimensional integration over n_y and n_z will not be carried out in the present work. Instead, the integration in the n_y direction is replaced by an effective spectral width, the integration over n_z carried out, and the total power integral estimated by the product of the effective width and the integration over n_z.

We consider the 6×1 slow wave array with the standard density profile and the array face 3 cm outside the limiter. Assuming that the 10 cm of plasma in front of the array constitutes the coupling region, waves with $|n_z| < 1.62$ are either evanescent or trapped in the coupling region. With 90° phasing, most of the incident power is in $1.25 \lesssim n_z \lesssim 3.25$, so that not much power is expected to be trapped in the outer part of the plasma. Our computation indicates that $\sim 9\%$ of the incident power is unable to escape the coupling region, while the reflection coefficient of the array may be read from Fig. 10: $|R|^2 \simeq 60\%$. The power spectrum $P_x(x = x_{right}, n_y = 0, n_z)$ for this case is plotted in Fig. 14, where we have taken $P_{inc} = 100$ kW. We have also shown the spectra at $x = x_{right}$ obtained when the array is 1 cm and 5 cm outside the limiter. As expected from Fig. 10, more power is coupled to the plasma as the array is pulled back. We also find that for this array, virtually no energy that escapes the coupling region is on the fast wave branch.

Finally, we consider the spectrum launched by the 4×3 fast wave array. At toroidal phasing of 90°, the primary peak in the incident power spectrum is centered on $n_z^{peak} = 1.01$, with a half-width-at-half-maximum of $(\Delta n_z)_{HWHM} \simeq 0.65$. With the standard density profile and the array face 3 cm outside the limiter, it is apparent that a very large fraction of the incident power will be trapped in the coupling region. In fact, our computation indicates that $\sim 70\%$ of the incident power is lost in this way, though the reflection coefficient of the array (with the poloidal phasing of $-70°$) is only 18% (see Fig. 6). Only $\lesssim 15\%$ of the incident power is able to escape the coupling region. Toroidally phasing the array at 180°, thus moving the peak to $n_z^{peak} = 2.02$ while maintaining the $-70°$ poloidal phasing to keep the reflection coefficient low, should eliminate the accessibility problem, and indeed we find that $\lesssim 10\%$ of the incident power is inaccessible in this case.

We show the power spectrum $P_x(x = x_{right}, n_y = -0.878, n_z)$ for the 4×3 fast wave array phased 90° toroidally and $-70°$ poloidally in Fig. 15. The value of n_y is chosen so that the path $n_y = -0.878$ runs along the peak of the spectrum for this poloidal phasing. Again, we show the spectrum for three array positions: 1 cm, 3 cm, and 5 cm outside the limiter. The Poynting flux at $x = x_{right}$ is split up between fast and slow waves, and we show their spectra separately. On the order of 20–40% of the power that actually escapes the coupling region is on the slow wave branch of the dispersion relation. The fact that the primary peak of the incident power spectrum is almost entirely inaccessible has an interesting consequence for current drive experiments: the array phasing in this example directs the power towards positive z, but the directivity of the spectrum that reaches the plasma core is 0.75 towards negative z for the case with the array face 3 cm outside the limiter. Assuming that very little current drive results from the dissipation of the power trapped in the cold coupling region plasma, this yields the easily tested prediction that under these conditions, any wave driven currents should flow in the 'wrong' direction.

Since the fast wave spectrum is cut off above a critical $|n_z|$ (which also depends on $|n_y|$), the mechanism of Ref. 17 for filling the spectral gap may not exist for pure fast wave current drive. In this case, the slow waves also launched by a realistic array may be important for this reason, while this parasitically launched slow wave power is likely to complicate any experimental investigation of any density limit for fast wave current drive [1].

By employing 180° toroidal phasing to alleviate the accessibility problem, the directivity of the spectrum is of course lost. Furthermore, raising the toroidal field lowers the minimum accessible $|n_z|$ but raises the reflection coefficient, as in Fig. 13. Clearly, an optimal toroidal field and toroidal phase angle between 90° and 180° exists, at which a reasonably large fraction of the incident power is able to reach the plasma core while retaining the maximum directivity. However, detailed optimization of the array and plasma parameters for current drive experiments is left to future work.

4. SUMMARY AND CONCLUSIONS

The algorithm of Bers and Theilhaber [14] has been numerically implemented and extended, resulting in a group of computer codes which have been used to study plasma–waveguide array coupling. The codes can evaluate both reflection coefficients and the launched power spectrum. When the guides are oriented with their long edges perpendicular to the toroidal field (slow wave launcher), good agreement is found between these codes and previously reported, less general codes. However, for high plasma densities in the vicinity of the coupler or for very low toroidal field strengths, accessibility becomes a problem in the coupling region, and the older codes become invalid for incident spectra with significant energy near $|n_x| = 1$. Under these conditions, lower reflection coefficients may be obtained with arrays oriented with the long edges of the guides parallel to the toroidal direction (fast wave launcher). To obtain these relatively low reflection coefficients, the array must be phased in the poloidal direction. Theilhaber and Bers [11] assumed that $n_y = 0$, and could not treat the effect of poloidal phasing, while the method of Refs. 12 and 13, wherein the launcher is idealized as launching a single plane wave with fixed (n_y, n_z), could not treat the up–down phasing asymmetry that exists even for a uniform plasma. This phenomenon, which arises from the matching of the plasma fields onto those of a realistic antenna model, appears to cause most of the up–down asymmetry evident in Fig. 8, for example. With a high (but not unreasonably so) edge density and the proper poloidal phasing, reflection coefficients lower than $|R|^2 \sim 20\%$ are found.

However, study of the power spectrum of the waves which actually escape the coupling region shows that only a small fraction of the incident power is delivered to the core of the plasma. As the peak of the spectrum approaches $n_x^{peak} \simeq 1$ to maximize current drive efficiency, a large fraction of the power is trapped in the outermost part of the plasma, particularly under the high density and low toroidal field conditions necessary to obtain lower reflection coefficients for the fast wave array. The effect on confinement of such large amounts of power being dissipated in the cold, collisional outermost layer of the plasma

is unclear, apart from the fact that little of the power from the rf source is actually transferred to the hot core of the plasma. For fast wave current drive experiments, a compromise will have to be found among the requirements of low array reflection coefficient, a spectrum characterized by high phase velocity and high directivity, and a large amount of power delivered to the plasma core. The incorporation of tuning elements into the array may help in this endeavor, by permitting a larger reflection coefficient.

ACKNOWLEDGMENTS

We thank Dr. J. Stevens for useful discussions.

This work was supported by U. S. Department of Energy Contract No. DE–AC02–76CHO3073.

References

[1] WÉGROWE, J., Fusion Technol. 7 (1985) 250.

[2] PORKOLAB, M., Lower Hybrid Heating Experiments in Tokamaks: An Overview, Massachusetts Institute of Technology Rep. PFC/CP–85–9 (Oct. 1985).

[3] INTOR Panel Proc., Phase 2A, Part I, IAEA, Vienna (1983) 167.

[4] BRAMBILLA, M., Nucl. Fusion **16** (1976) 47.

[5] STEVENS, J., ONO, M., HORTON, R., WILSON, J. R., Nucl. Fusion **21** (1981) 1259.

[6] BOLEY, C.D., Grill: A Code to Calculate the Spectrum of Lower–Hybrid Waves Launched by a Brambilla Waveguide Array, ANL/FPP/TM–135 (June 1980).

[7] In the cold plasma approximation, the WKB dispersion relation is a bi-quadratic, yielding two physically distinct roots for k_x for a given (k_y, k_z). Though both roots are represented by one wave–normal surface on a CMA diagram [19] and hence, in one sense, cannot be considered two separate 'slow' and 'fast' roots, we shall adhere to another convention [14] and refer to the solution with larger k_x^2 as the "slow wave" and to the other as the "fast" wave. The slow wave in the LHRF is also sometimes referred to as the "lower hybrid wave;" the fast wave is sometimes called the "whistler" or "fast Alfvén wave."

[8] GORMEZANO, C., MOREAU, D., Plasma Phys. and Controlled Fusion **26** (1984) 553.

[9] STEVENS, J. E., BERNABEI, S., BUDNY, R., HOOKE, W. M., *et al.*, Bull. Am. Phys. Soc. **26** (1981) 974.

[10] BRAMBILLA, M., Nucl. Fusion **19** (1979) 1343.

[11] THEILHABER, K., BERS, A., Nucl. Fusion **20** (1980) 547.

[12] BERGER, R. L., PERKINS, F. W., TROYON, F., Coupling of Slow and Fast Waves to Plasmas Near the Lower Hybrid Frequency, Princeton Plasma Physics Lab. Rep. PPPL–1366 (Aug. 1977).

[13] McWILLIAMS, R., MOK, Y., Fusion Technol. **7** (1985) 283.

[14] BERS, A.,THEILHABER, K. S., Nucl. Fusion **23** (1983) 41.

[15] FORTGANG, C. M., COLESTOCK, P. L., HWANG, D. Q., in Course and Workshop on Applications of RF Waves to Tokamak Plasmas (Int. School of Plasma Phys., Varenna, Italy, Sept. 5–14, 1985), to be published.

[16] COLESTOCK, P. L., STEVENS, J. E., HOSEA, J. C., WILSON, J. R., PINSKER, R., FORTGANG, C. M., in RF Plasma Heating (Proc. 6th Top. Conf., Callaway Gardens, GA, 1985) AIP, New York (1985) 48.

[17] DECYK, V., ABE, H., Current Drive with Fast Phase Velocity Lower Hybrid Waves, UCLA Rep. PPG–890 (Sept. 1985).

[18] SHAMPINE, L. F., GORDON, M. K., Computer Solution of Ordinary Differential Equations, W. H. Freeman and Co., San Francisco (1975).

[19] STIX, T.H., The Theory of Plasma Waves, McGraw–Hill, New York (1962).

[20] BRAMBILLA, M., Review of the Grill Theory, Association Euratom–CEA Rep. EUR–CEA–FC 890 (April 1977).

[21] BERNABEI, S., DAUGHNEY, C., EFTHIMION, P., HOOKE, W., *et al.*, Phys. Rev. Lett. **49** (1982) 1255.

[22] SKIFF, F., Linear and Non–linear Excitation of Slow Waves in the Ion Cyclotron Frequency Range, Ph. D. dissertation, Princeton University (1985).

Figures

Fig. 1. The general array configuration and the coordinate system employed.

Fig. 2. Illustrating the contour dictated by causality in the complex k_z plane.

Fig. 3. Comparison of Stevens code [5] results with present work: individual guide reflection coefficients as a function of phase angle.

Fig. 4. Comparison of Stevens code results with present work: net transmission coefficient for 4–guide array as a function of phase angle.

Fig. 5. The density profile used for the fast wave array example. The nominal position of the waveguide array face is marked with an arrow.

Fig. 6. Power reflection coefficient for the fast wave array as a function of the distance between the array face and the limiter for two poloidal phasings.

Fig. 7. (a) Power reflection coefficient for the standard case as a function of poloidal phasing angle, with the toroidal phase angle = 90°.

(b) Power reflection coefficient for the standard case as a function of toroidal phasing angle, with the poloidal phase angle = 0°.

(c) Power reflection coefficient for the standard case as a function of toroidal phasing angle, with the poloidal phase angle = −90°.

Fig. 8. Contours of power reflection coefficient for arbitrary uniform phasings for the standard case.

Fig. 9. Contours of power reflection coefficient for uniform plasma with $n_e = 1.1 \times 10^{12}$ cm^{-3} , $B_0 = 20$ kG.

Fig. 10. Power reflection coefficient for the 6 × 1 slow wave array as a function of the distance between the array face and the limiter. 'Standard' density profile (see Fig. 5), $B_0 = 20$ kG, toroidal phase angle of 90°.

Fig. 11. Comparison of reflection coefficients for the 4 × 3 fast wave array and the 6 × 1 slow wave array as a function of toroidal phase angle. 'Standard'

density profile, array faces 3 cm outside the limiter, $B_0 = 20$ kG. For the fast wave array, the poloidal phase angle is $-70°$.

Fig. 12. Power reflection coefficient for the 6×1 slow wave array as a function of toroidal field strength B_0. 'Standard' density profile, array face 3 cm outside the limiter, toroidal phase angle is 90°.

Fig. 13. Power reflection coefficient for the 4×3 fast wave array as a function of toroidal field strength B_0. 'Standard' density profile, array face 3 cm outside the limiter, toroidal phase angle is 90°.

Fig. 14. The Fourier transform of the Poynting flux in the x–direction at $x = x_{right}$, along $n_y = 0$, as a function of n_z. 6×1 slow wave array with 90° toroidal phasing angle, 'standard' density profile, array face 1 cm (dashed line), 3 cm (solid line), and 5 cm (dotted line) outside the limiter. Total incident power $P_{inc} = 100$ kW.

Fig. 15. The Fourier transform of the Poynting flux in the x–direction at $x = x_{right}$, along $n_y = -0.878$, as a function of n_z. 4×3 fast wave array with 90° toroidal phasing angle, $-70°$ poloidal phasing angle, 'standard' density profile, array face 1 cm (dashed line), 3 cm (solid line), and 5 cm (dotted line) outside the limiter. Total incident power $P_{inc} = 100$ kW.

#86X0216

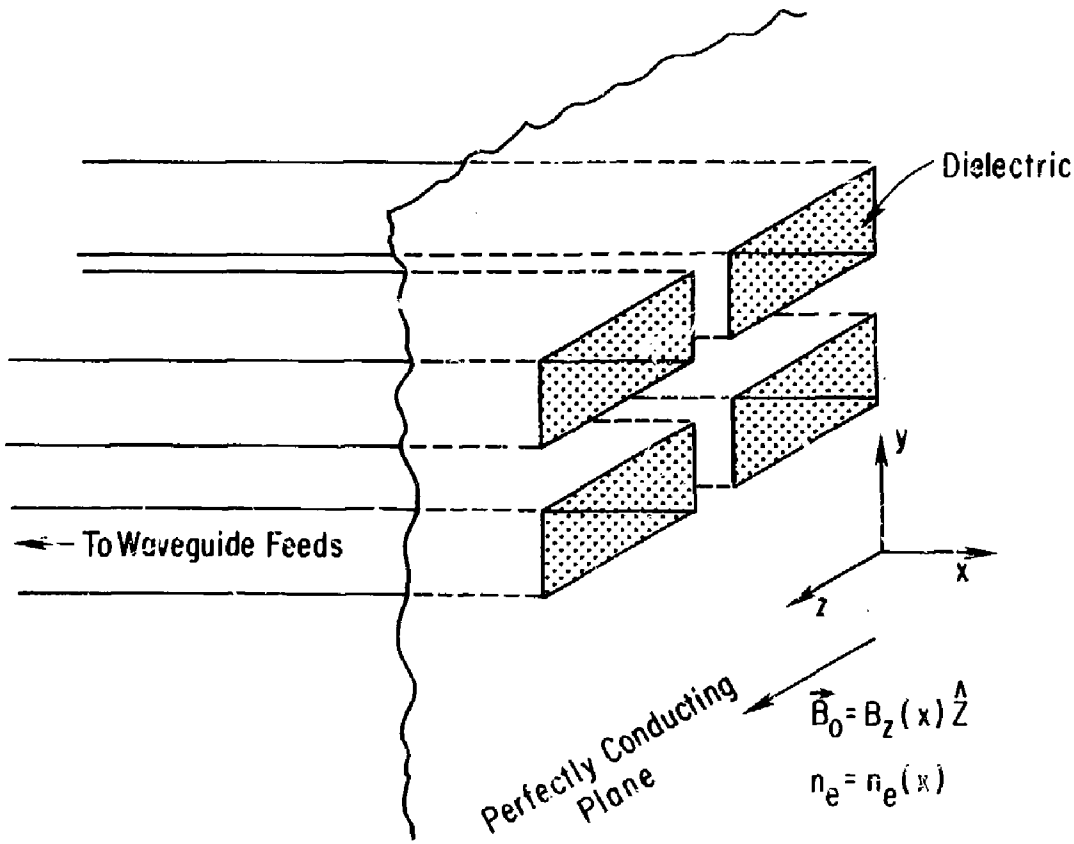

Fig. 1

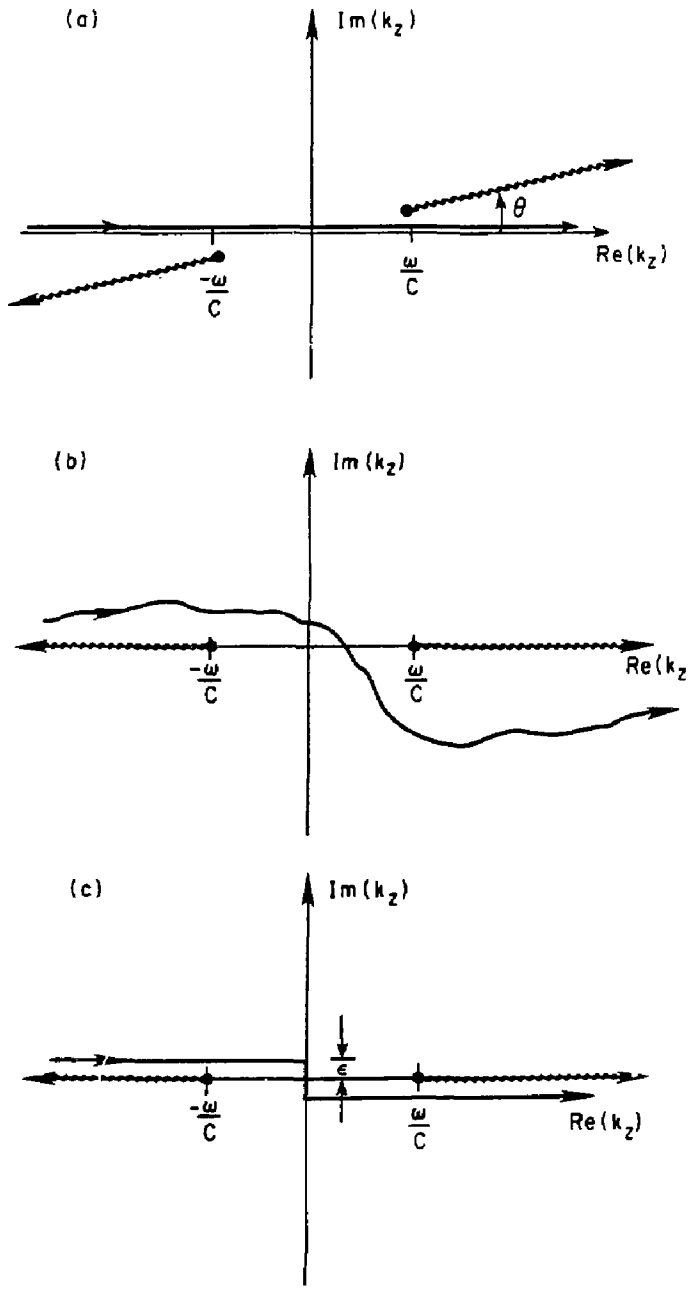

Fig. 2

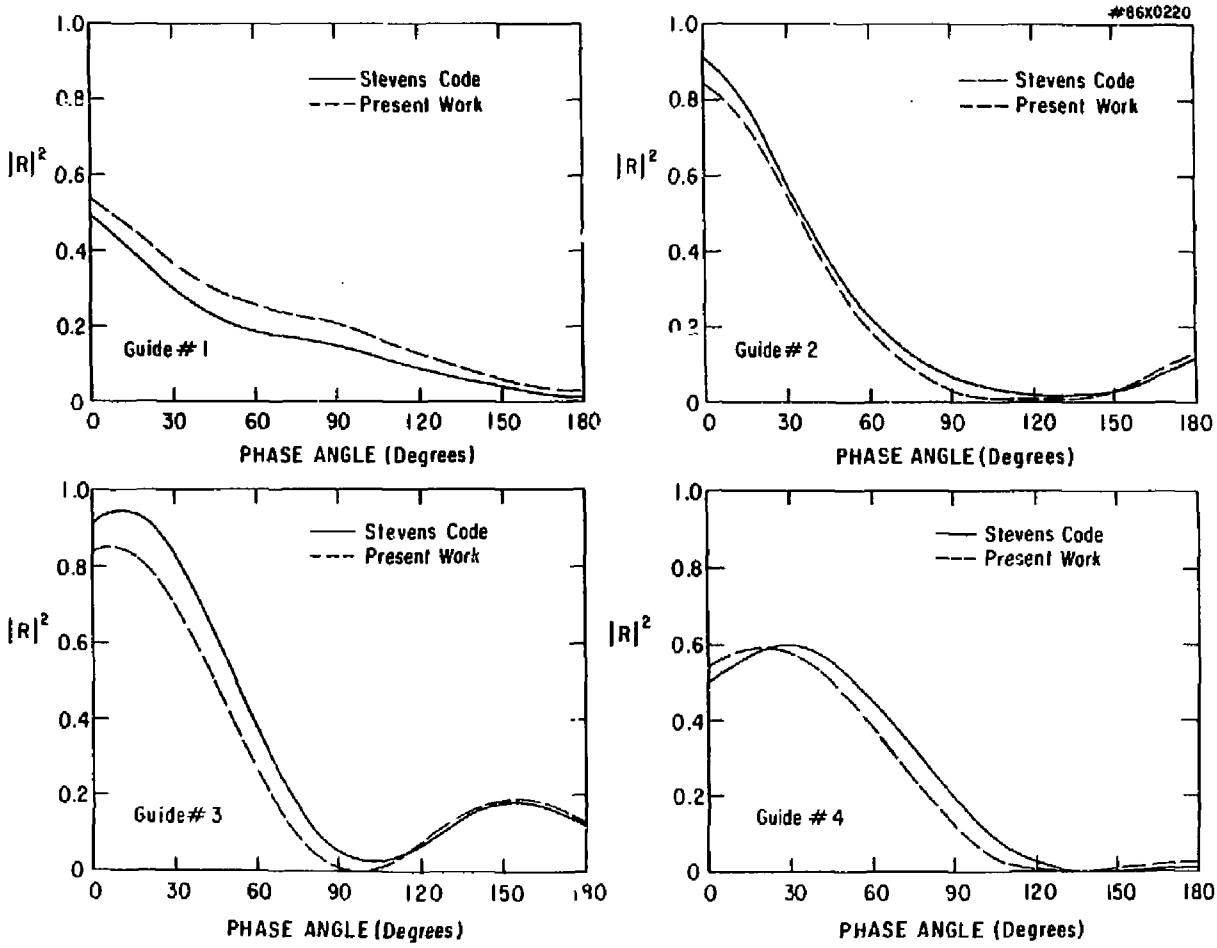
#86X0220
Stevens Code
Present Work
$|R|^2$
Guide # 1
Guide # 2
Guide # 3
Guide # 4
PHASE ANGLE (Degrees)
0
0.2
0.4
0.6
0.8
1.0
30
60
90
120
150
180

Fig. 3

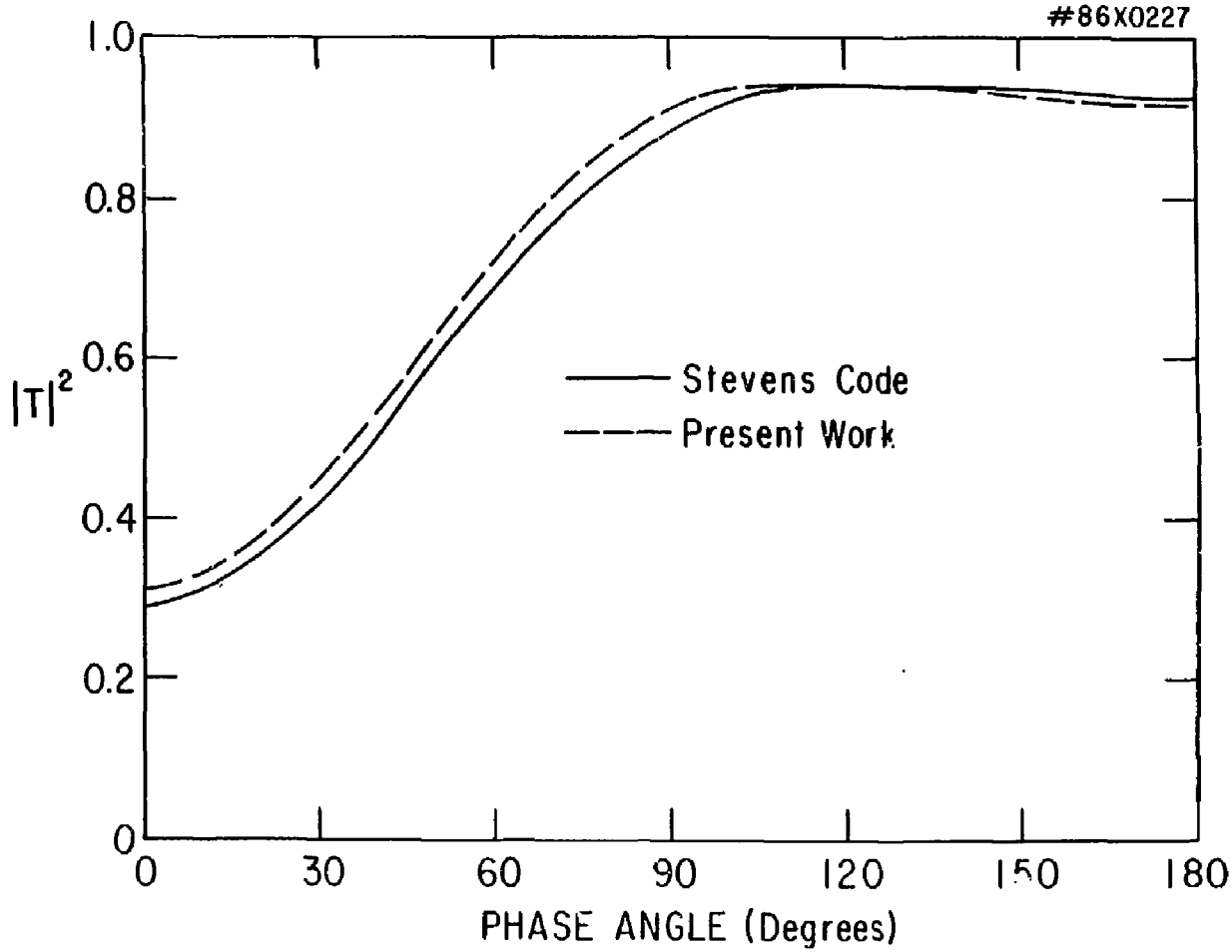
#86X0227
1.0
0.8
0.6
0.4
0.2
0
$|T|^2$
Stevens Code
Present Work
0
30
60
90
120
150
180
PHASE ANGLE (Degrees)

Fig. 4

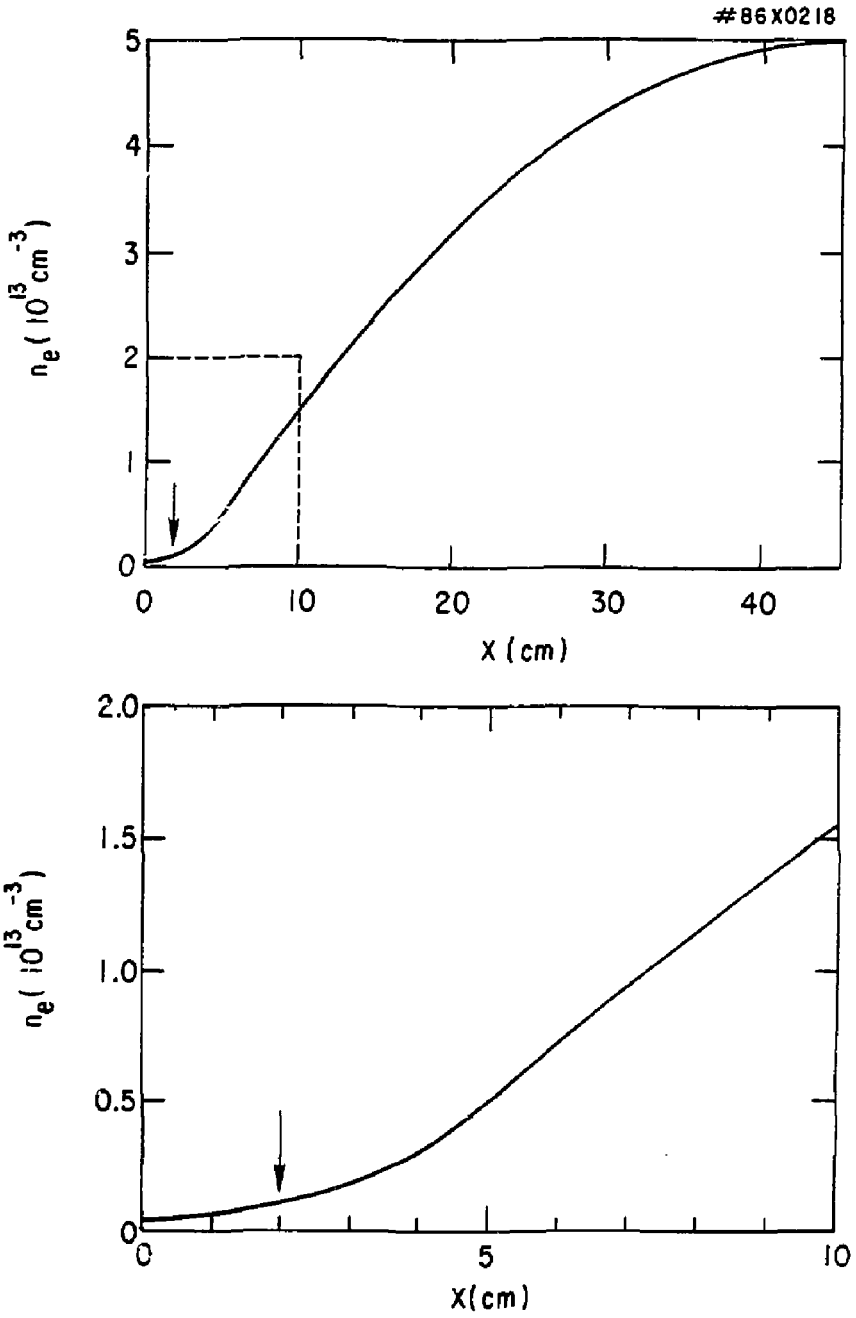
#86X0218
5
4
3
2
1
0
$n_e(10^{13}cm^{-3})$
0
10
20
30
40
X (cm)
2.0
1.5
1.0
0.5
0
$n_e(10^{13}cm^{-3})$
0
5
10
X(cm)

Fig. 5

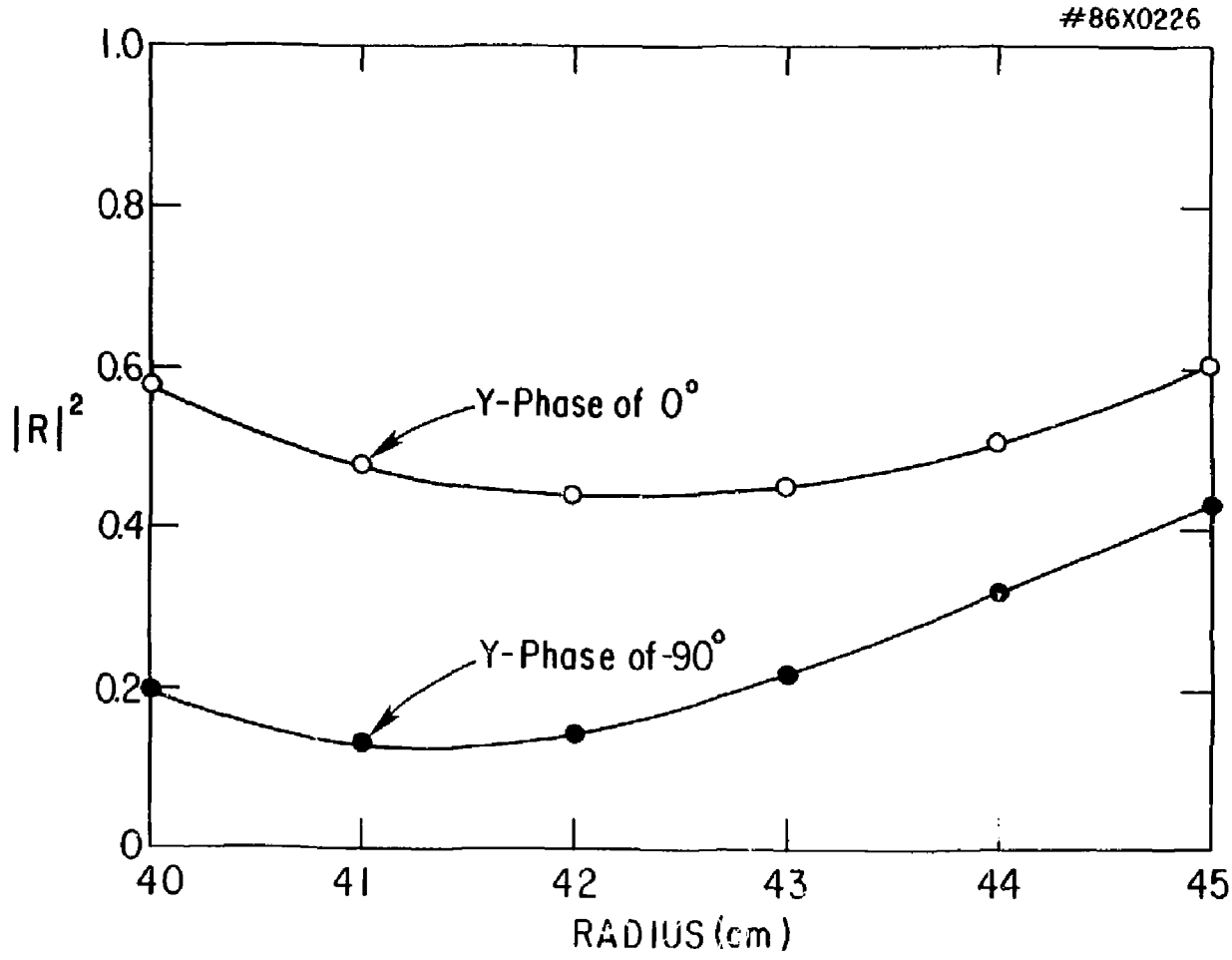
#86X0226
1.0
0.8
0.6
0.4
0.2
0
$|R|^2$
Y-Phase of 0°
Y-Phase of -90°
40
41
42
43
44
45
RADIUS (cm)

Fig. 6

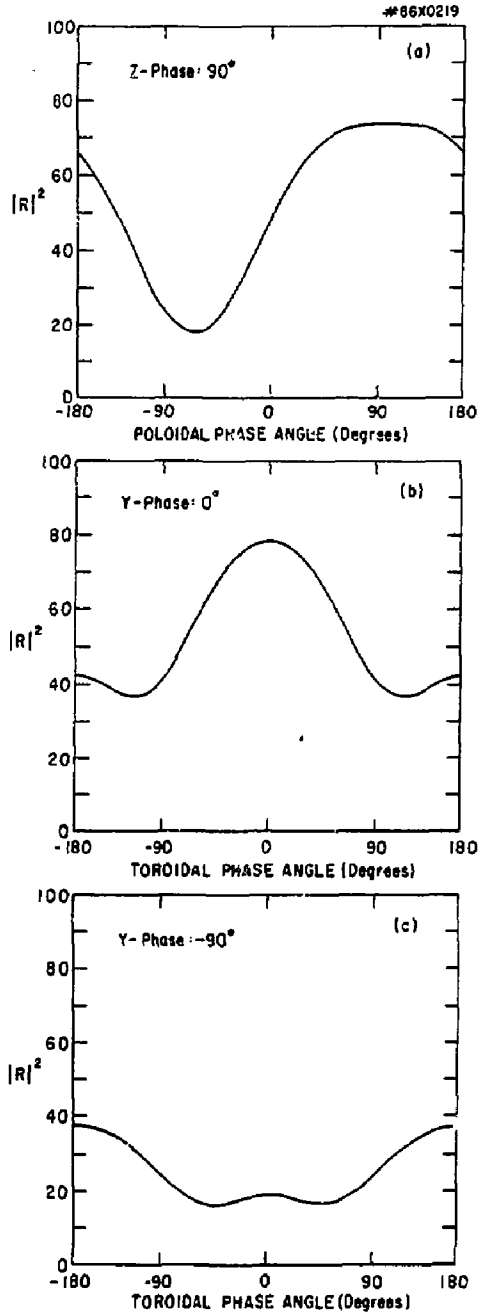
#86X0219
(a)
Z-Phase: 90°
100
80
60
40
20
0
$|R|^2$
-180
-90
0
90
180
POLOIDAL PHASE ANGLE (Degrees)
(b)
Y-Phase: 0°
TOROIDAL PHASE ANGLE (Degrees)
(c)
Y-Phase: -90°
TOROIDAL PHASE ANGLE (Degrees)

Fig. 7

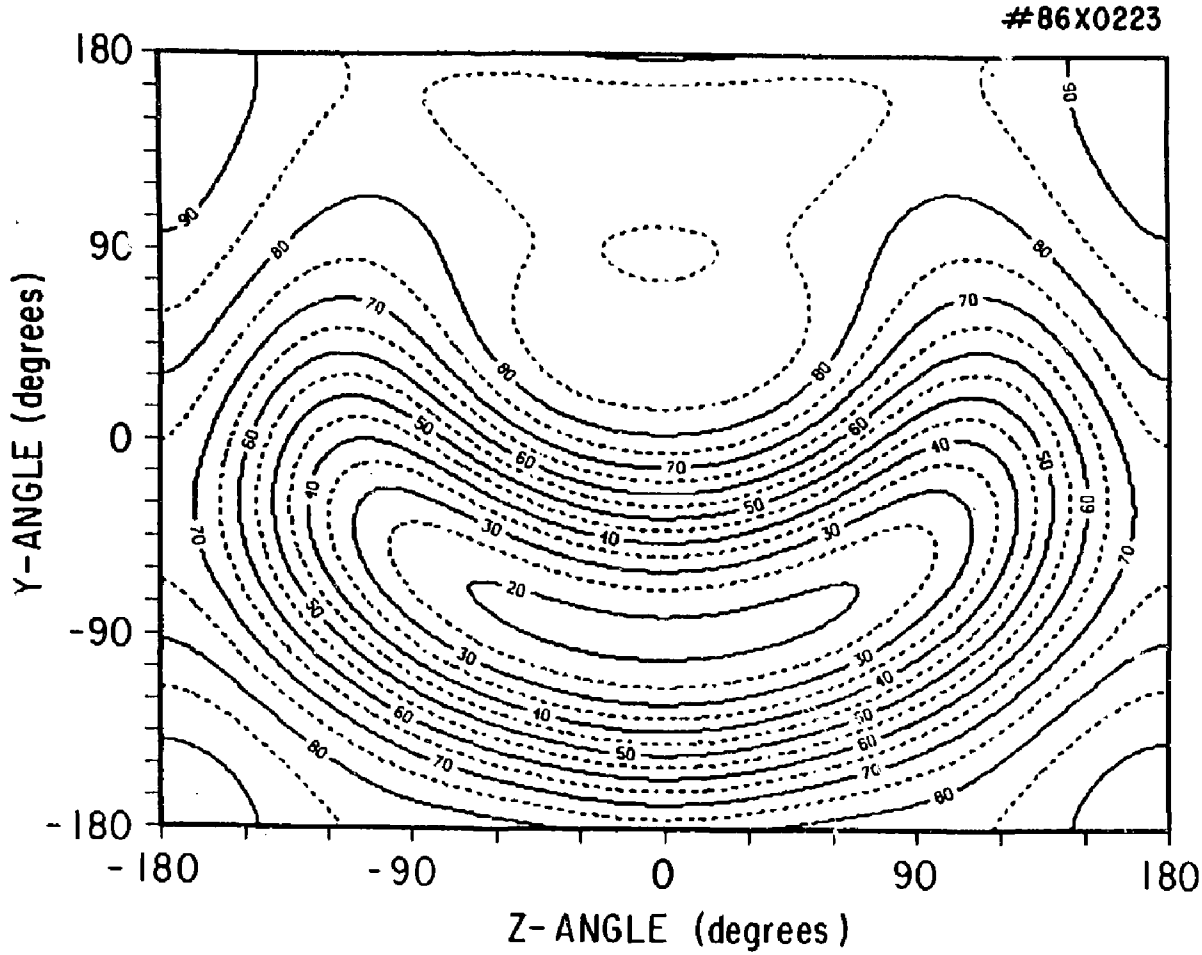
#86X0223
180
90
0
-90
-180
Y-ANGLE (degrees)
-180
-90
0
90
180
Z-ANGLE (degrees)

Fig. 8

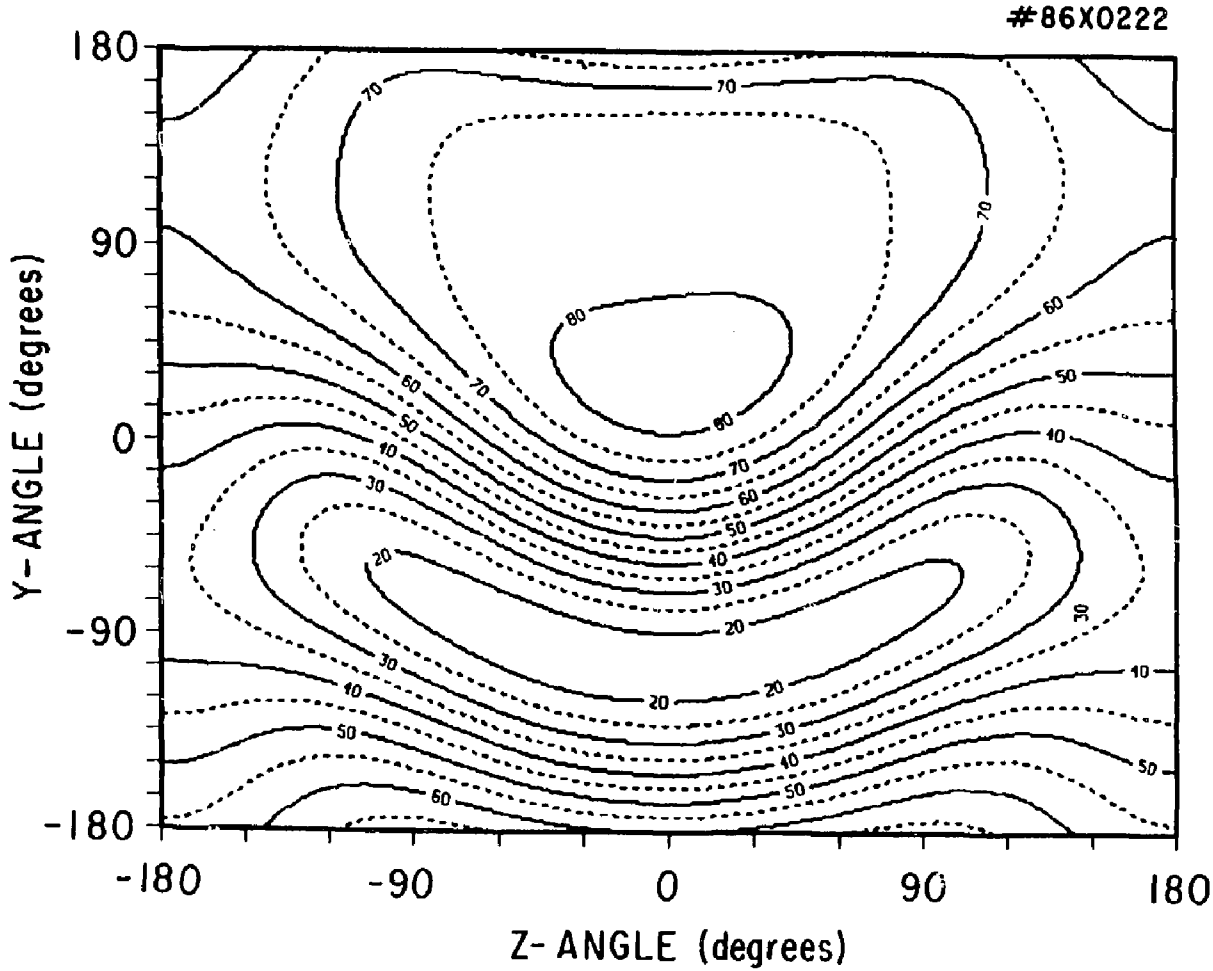
#86X0222
180
90
0
-90
-180
Y-ANGLE (degrees)
-180
-90
0
90
180
Z-ANGLE (degrees)
70
60
50
40
30
20
80

Fig. 9

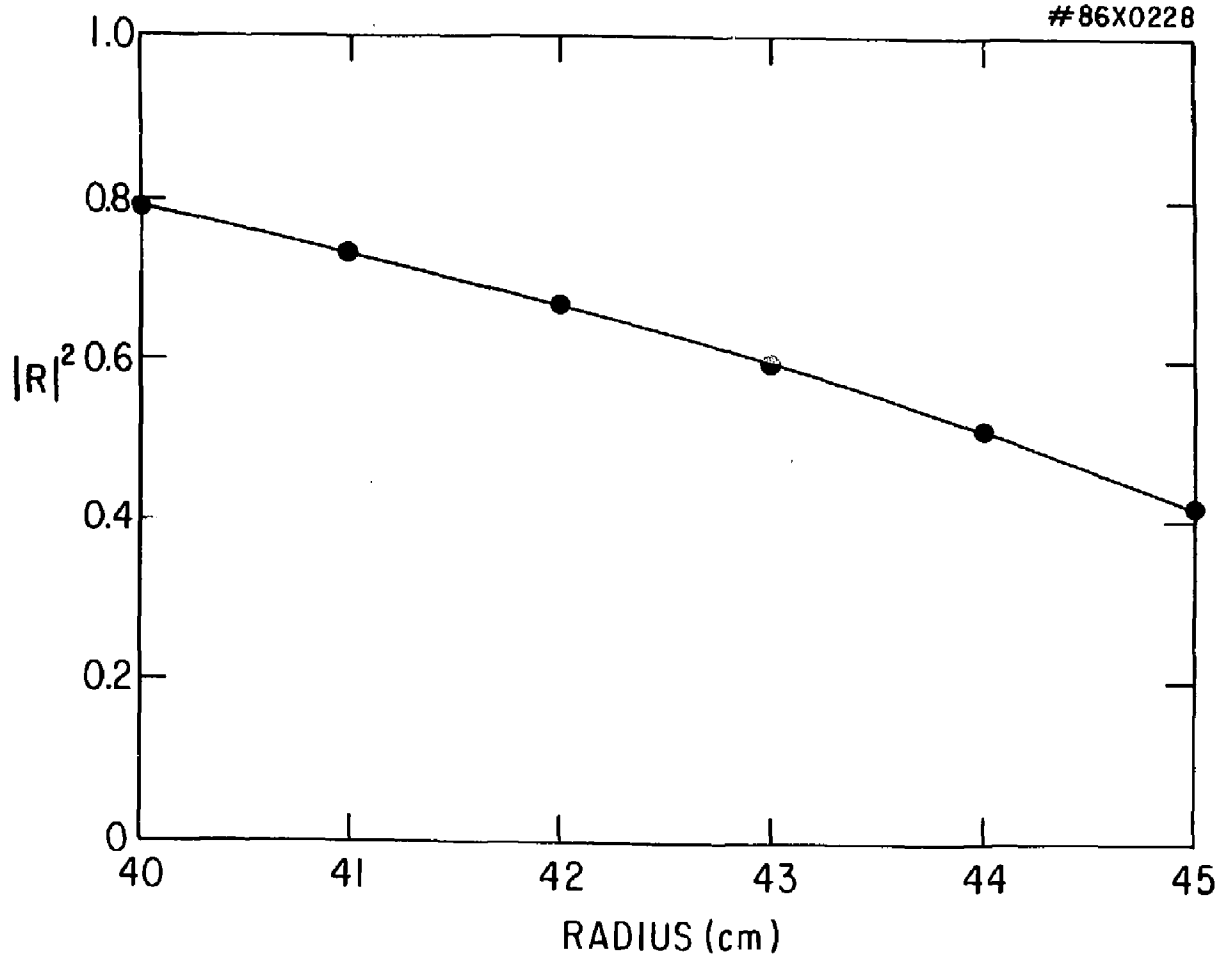

Fig. 10

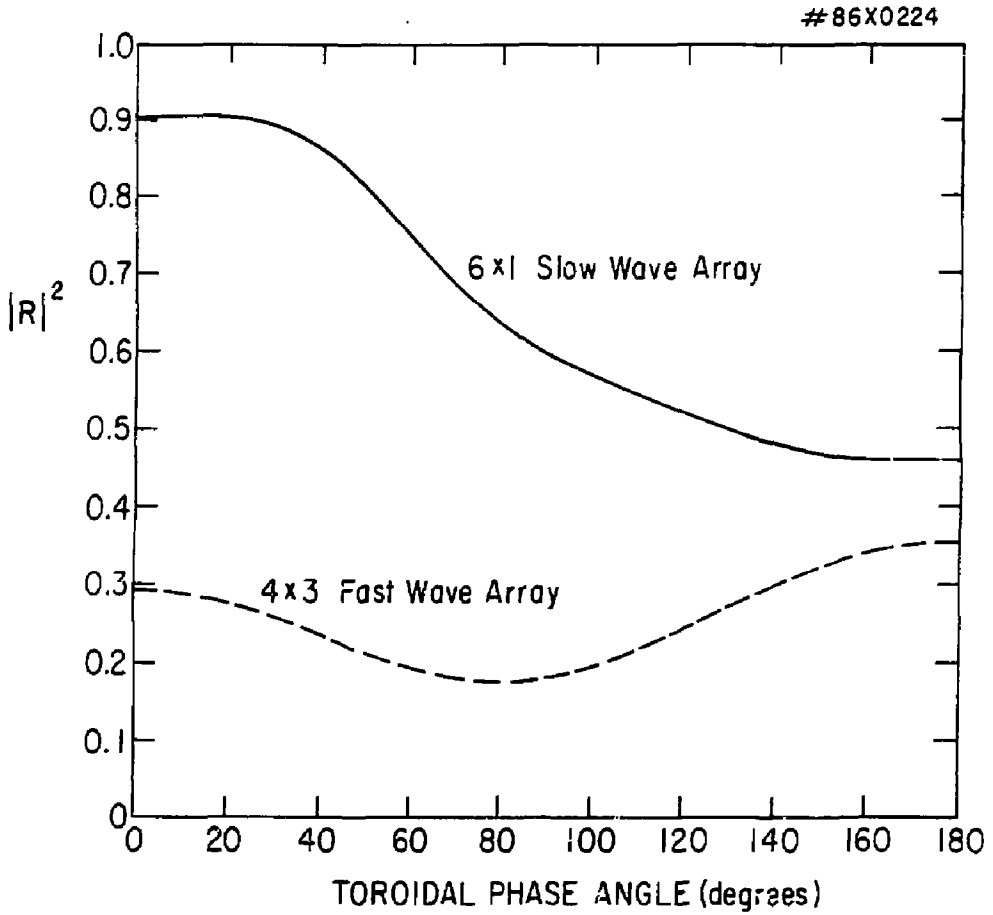
#86X0224
1.0
0.9
0.8
0.7
0.6
0.5
0.4
0.3
0.2
0.1
0
$|R|^2$
6x1 Slow Wave Array
4x3 Fast Wave Array
0
20
40
60
80
100
120
140
160
180
TOROIDAL PHASE ANGLE (degrees)

Fig. 11

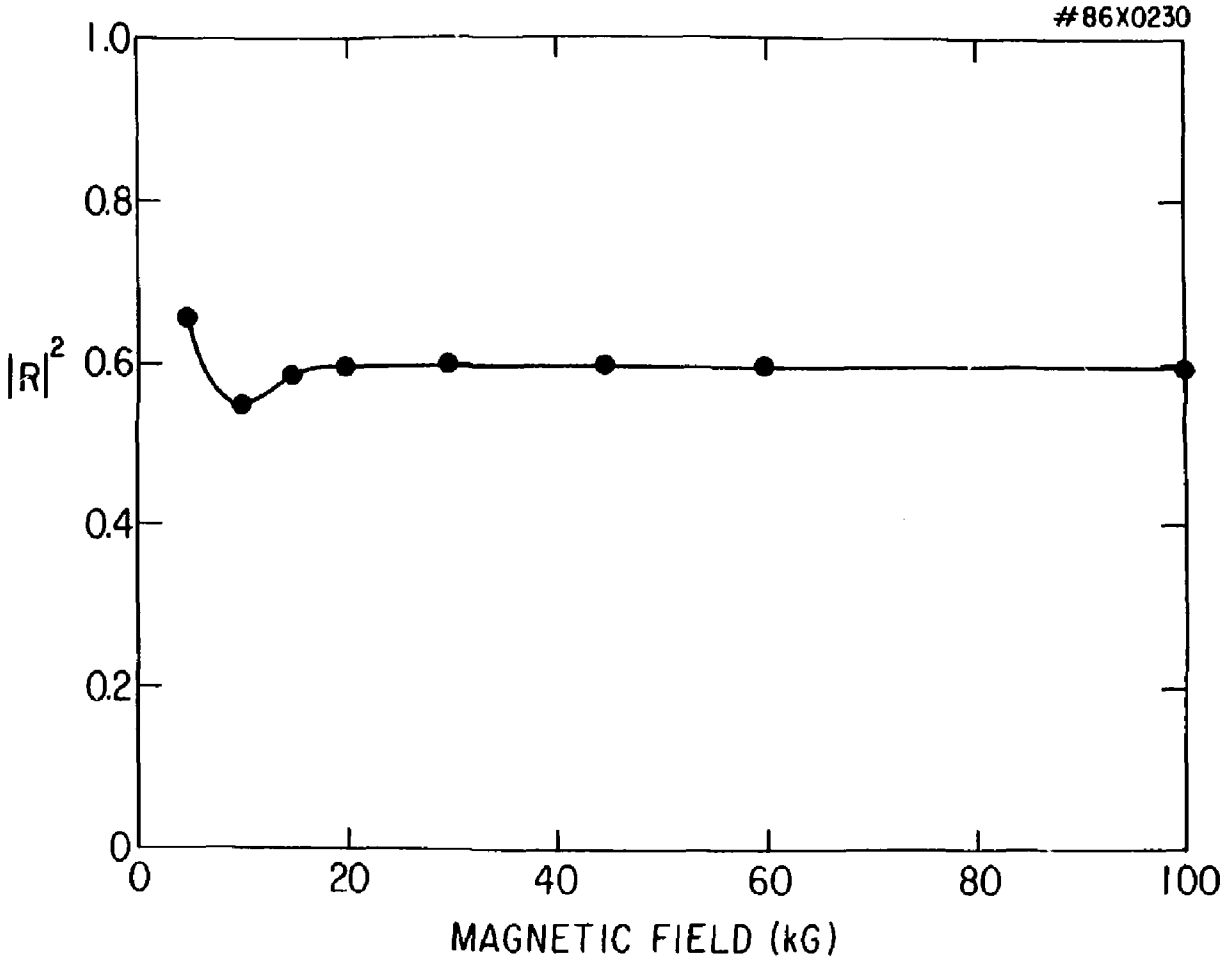

Fig. 12

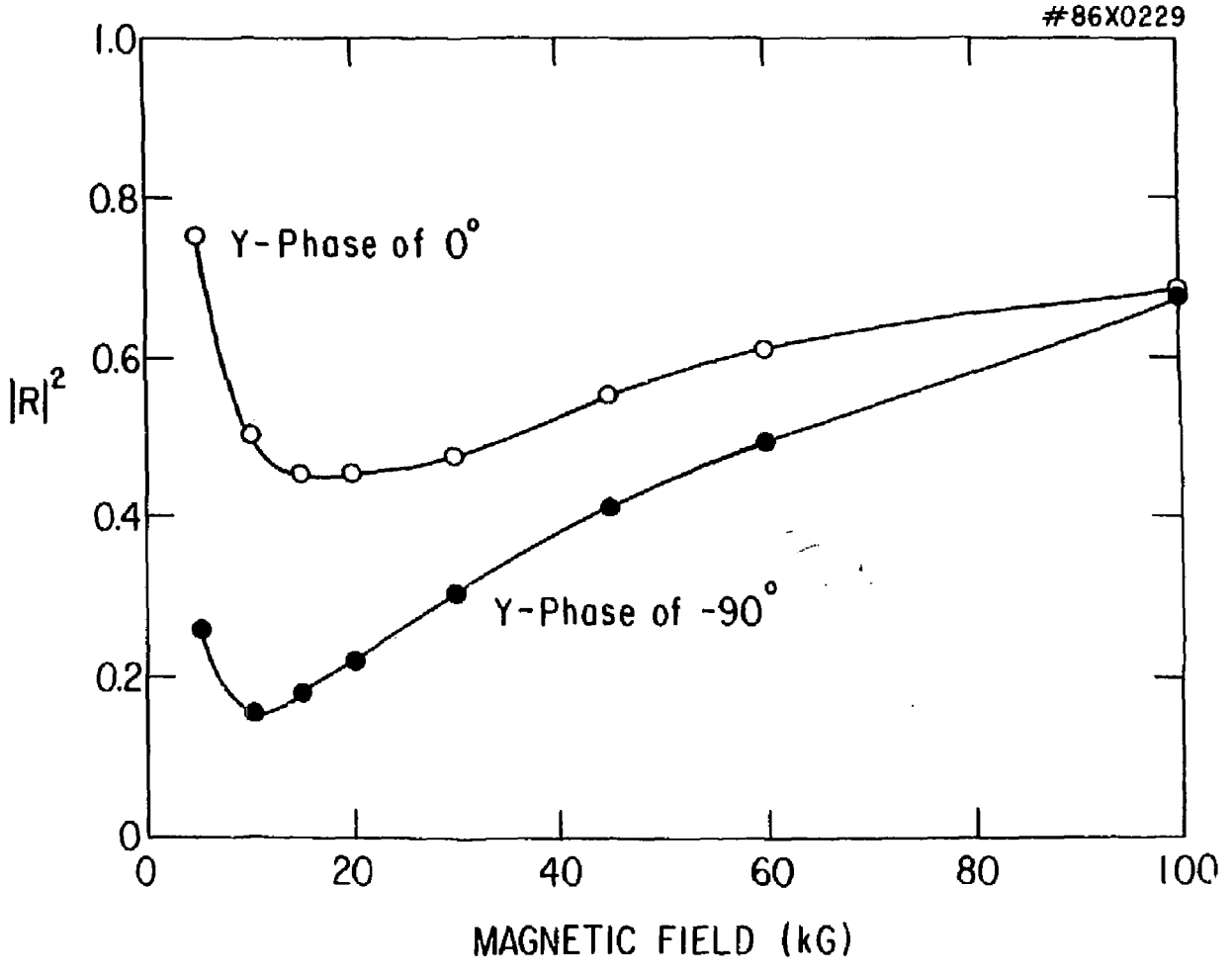
#86X0229
1.0
0.8
0.6
0.4
0.2
0
$|R|^2$
Y-Phase of 0°
Y-Phase of -90°
0
20
40
60
80
100
MAGNETIC FIELD (kG)

Fig. 13

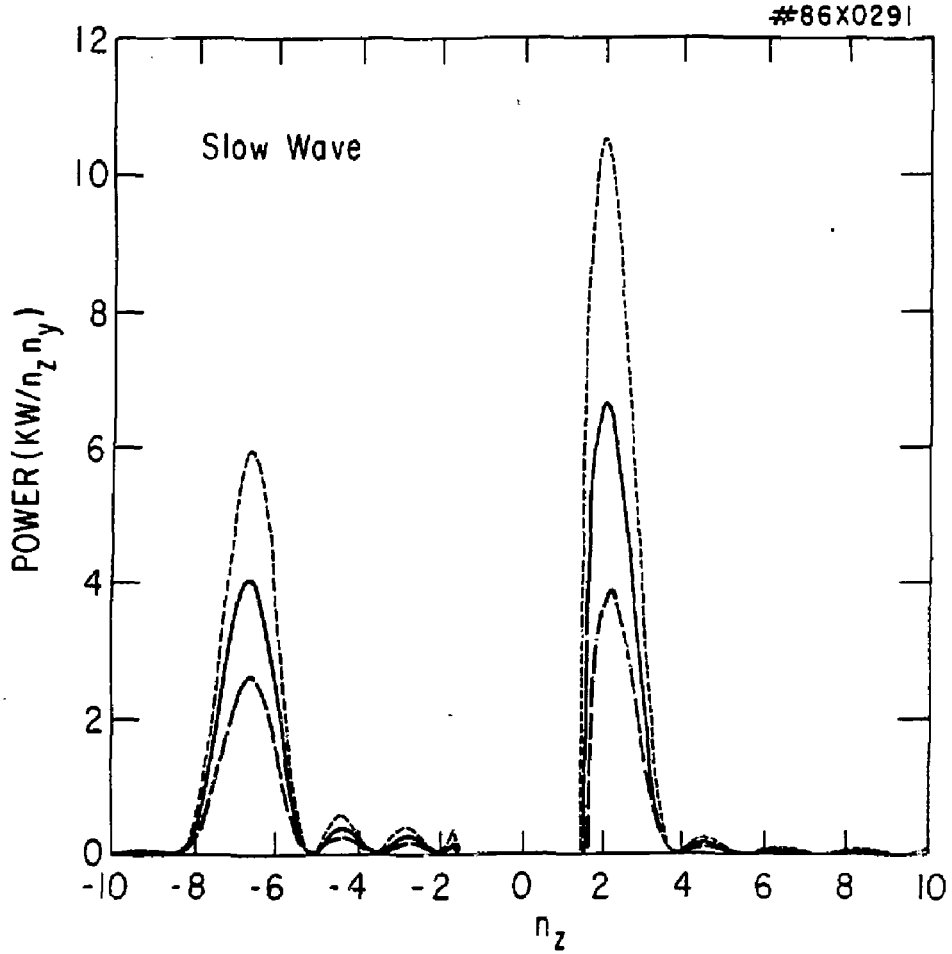
#86X0291
Slow Wave
POWER (KW/$n_z n_y$)
12
10
8
6
4
2
0
-10
-8
-6
-4
-2
0
2
4
6
8
10
n_z

Fig. 14

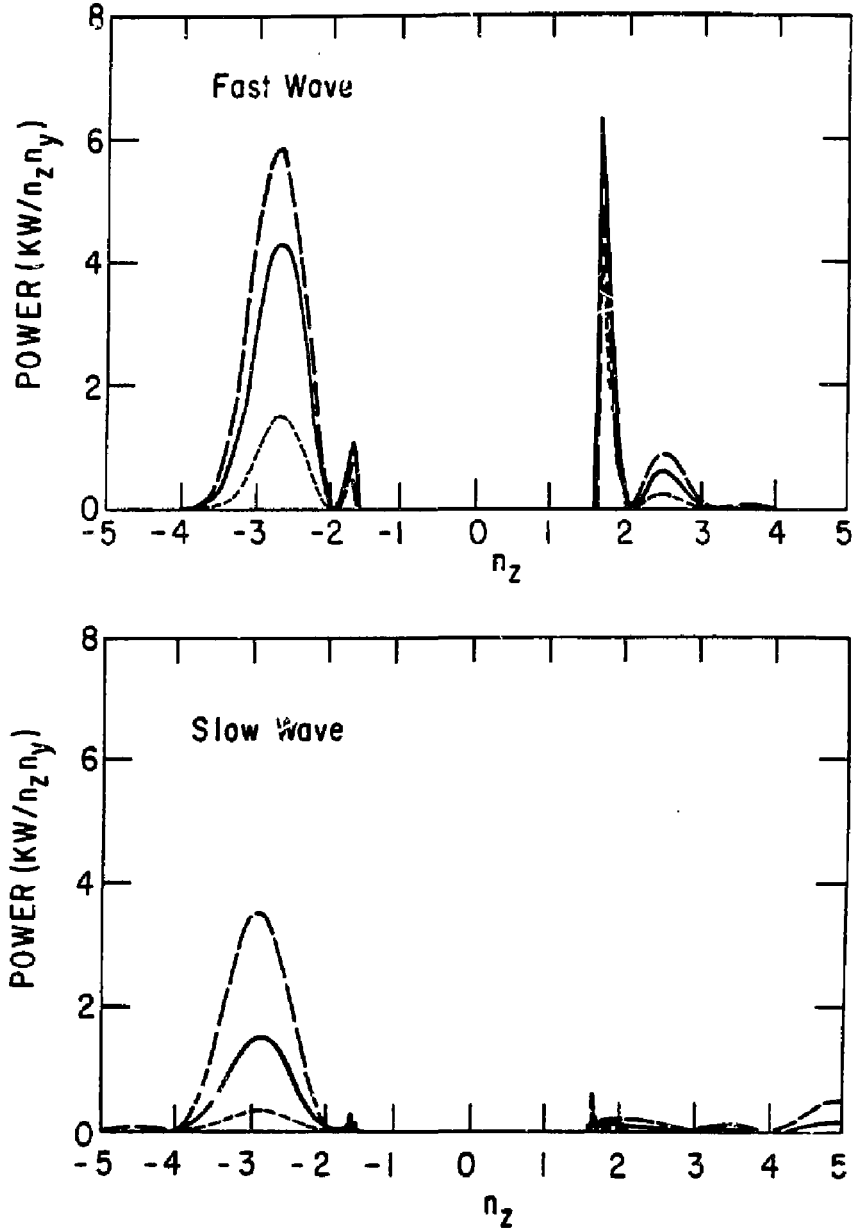

Fig. 15

EXTERNAL DISTRIBUTION IN ADDITION TO UC-20

Plasma Res Lab, Austra Nat'l Univ, AUSTRALIA
Dr. Frank J. Paoloni, Univ of Wollongong, AUSTRALIA
Prof. I.R. Jones, Flinders Univ., AUSTRALIA
Prof. M.H. Brennan, Univ Sydney, AUSTRALIA
Prof. F. Cap, Inst Theo Phys, AUSTRIA
Prof. Frank Verheest, Inst theoretische, BELGIUM
Dr. D. Palumbo, Dg XII Fusion Prog, BELGIUM
Ecole Royale Militaire, Lab de Phys Plasmas, BELGIUM
Dr. P.H. Sakanaka, Univ Estadual, BRAZIL
Dr. C.R. James, Univ of Alberta, CANADA
Prof. J. Teichmann, Univ of Montreal, CANADA
Dr. H.M. Skarsgard, Univ of Saskatchewan, CANADA
Prof. S.R. Sreenivasan, University of Calgary, CANADA
Prof. Tudor W. Johnston, INRS-Energie, CANADA
Dr. Hannes Barnard, Univ British Columbia, CANADA
Dr. M.P. Bachynski, MPB Technologies, Inc., CANADA
Chalk River, Nucl Lab, CANADA
Zhengwu Li, SW Inst Physics, CHINA
Library, Tsing Hua University, CHINA
Librarian, Institute of Physics, CHINA
Inst Plasma Phys, Academia Sinica, CHINA
Dr. Peter Lukac, Komenskeho Univ, CZECHOSLOVAKIA
The Librarian, Culham Laboratory, ENGLAND
Prof. Schatzman, Observatoire de Nice, FRANCE
J. Radet, CEN-BP6, FRANCE
AM Dupas Library, AM Dupas Library, FRANCE
Dr. Tom Mual, Academy Bibliographic, HONG KONG
Preprint Library, Cent Res Inst Phys, HUNGARY
Dr. R.K. Chhajlani, Vikram Univ. INDIA
Dr. B. Dasgupta, Saha Inst, INDIA
Dr. P. Kaw, Physical Research Lab, INDIA
Dr. Phillip Rosenau, Israel Inst Tech, ISRAEL
Prof. S. Cuperman, Tel Aviv University, ISRAEL
Prof. G. Rostagni, Univ Di Padova, ITALY
Librarian, Int'l Ctr Theo Phys, ITALY
Miss Clelia De Palo, Assoc EURATOM-ENEA, ITALY
Biblioteca, del CNR EURATOM, ITALY
Dr. H. Yamato, Toshiba Res & Dev, JAPAN
Direc. Dept. Ig. Tokamak Dev. JAERI, JAPAN
Prof. Nobuyuki Inoue, University of Tokyo, JAPAN
Research Info Center, Nagoya University, JAPAN
Prof. Kyoji Nishikawa, Univ of Hiroshima, JAPAN
Prof. Sigeru Mori, JAERI, JAPAN
Prof. S. Tanaka, Kyoto University, JAPAN
Library, Kyoto University, JAPAN
Prof. Ichiro Kawakami, Nihon Univ, JAPAN
Prof. Satoshi Itoh, Kyushu University, JAPAN
Dr. D.I. Choi, Adv. Inst Sci & Tech, KOREA
Tech Info Division, KAERI, KOREA
Bibliotheek, Fom-Inst Voor Plasma, NETHERLANDS
Prof. B.S. Liley, University of Waikato, NEW ZEALAND
Prof. J.A.C. Cabral, Inst Superior Tecn, PORTUGAL
Dr. Octavian Petrus, Al. I. CUZA University, ROMANIA
Prof. M.A. Hellberg, University of Natal, SO AFRICA
Dr. Johan de Villiers, Plasma Physics, Nucor, SO AFRICA
Fusion Div. Library, JEN, SPAIN
Prof. Hans Wilhelmson, Chalmers Univ Tech, SWEDEN
Dr. Lennart Stenflo, University of UMEA, SWEDEN
Library, Royal Inst Tech, SWEDEN
Centre de Recherchesen, Ecole Polytech Fed, SWITZERLAND
Dr. V.T. Tolok, Kharkov Phys Tech Ins, USSR
Dr. D.D. Ryutov, Siberian Acad Sci, USSR
Dr. G.A. Eliseev, Kurchatov Institute, USSR
Dr. V.A. Glukhikh, Inst Electro-Physical, USSR
Institute Gen. Physics, USSR
Prof. T.J.M. Boyd, Univ College N Wales, WALES
Dr. K. Schindler, Ruhr Universitat, W. GERMANY
Nuclear Res Estab, Julich Ltd, W. GERMANY
Librarian, Max-Planck Institut, W. GERMANY
Bibliothek, Inst Plasmaforschung, W. GERMANY
Prof. R.K. Janev, Inst Phys, YUGOSLAVIA